

Final Report - Design, Fabrication and Analysis of Mach-Zender Interferometers in Silicon Photonics

Rafael Ribeiro (edX username: rafaribs99)

1. Introduction

Silicon photonics has emerged as a transformative technology, enabling the integration of optical components on silicon substrates. This integration leverages the mature CMOS fabrication processes, offering advantages such as reduced power consumption, compact device footprints, and cost-effective mass production. The compatibility with existing semiconductor manufacturing infrastructure makes silicon photonics a compelling platform for developing high-speed, low-power optical interconnects.

A fundamental component in silicon photonics is the Mach-Zehnder Interferometer (MZI), which serves as a versatile tool for manipulating light through interference. MZIs are widely used in applications like modulators, switches, and sensors due to their ability to precisely control phase and amplitude.

i. Objectives of the Course Project

The primary objective of this project is to design, simulate, and analyze various MZI configurations to understand their optical behavior and compare performance with expected response. The specific circuits designed and simulated were:

- Three MZIs with a path length difference (ΔL) of $25.44 \mu\text{m}$
- Two MZIs with $\Delta L = 100 \mu\text{m}$
- One MZI with $\Delta L = 402.62 \mu\text{m}$
- An MZI adjustable splitter with an 80%/20% power splitting, implemented using two adiabatic splitters with the second inverted
- A two-port MZI designed to measure signals from both paths and observe complementary outputs.

These configurations also aim to explore the impact of path length differences and splitter ratios on the interference patterns and overall device performance and check manufacturing variability with the repeatability of some of the devices.

2. Theory

i. Silicon Photonic Waveguides

In silicon photonics, waveguides are typically composed of a high-index silicon core ($n \approx 3.45$ at 1550 nm) embedded in a lower-index cladding such as silicon dioxide ($n \approx 1.44$), forming a strong optical confinement due to the large refractive index contrast. This high index contrast allows for tight mode confinement, enabling ultra-compact device geometries and sharp bends, albeit at the cost of increased sensitivity to fabrication imperfections and sidewall roughness.

Waveguides support guided optical modes, and each mode is characterized by an effective refractive index n_{eff} which represents the average refractive index "experienced" by the optical mode as it propagates through the structure. The group index (n_g), which governs the group velocity of a pulse traveling through the waveguide, incorporates the wavelength dependence of n_{eff} :

$$n_{eff} = n_{eff} - \lambda \frac{dn_{eff}}{d\lambda} \quad (1)$$

To quantify the chromatic dispersion of the waveguide, we use the dispersion parameter D, defined in units of $\frac{ps}{nm \cdot km}$, which measures how different wavelengths of light spread temporally due to group velocity differences:

$$D = -\frac{\lambda}{c} \cdot \frac{d^2 n_{eff}}{d\lambda^2} \quad (2)$$

In this project, a second-degree polynomial fit of the Taylor series is applied to the simulated n_{eff} vs. wavelength data, to obtain a compact model of the waveguide, and extract values of n_g and D from the fitting parameters. The exact expressions will be shown in section 3. Modelling and Simulation.

ii. Mach-Zehnder Interferometer (MZI)

The Mach-Zehnder Interferometer is one of the most widely used structures in integrated optics due to its simplicity and effectiveness in translating phase differences into intensity variations. The basic structure consists of two 3 dB optical splitters (typically implemented as directional couplers or multimode interferometers), with two arms in between that may have a path length difference or experience different phase shifts due to environmental or material changes.

When a monochromatic optical signal enters the MZI, it is split into two arms. If the optical path lengths are identical, the two beams recombine in phase, resulting in constructive interference at the output. However, if there is a difference in optical path length (ΔL), a relative phase shift is introduced, leading to interference that varies with wavelength.

The output intensity as a function of wavelength can be modelled as:

$$I_0 = \frac{1}{4} I_i \left| \left(e^{-j\beta_1 L_1 - \frac{\alpha_1}{2} L_1} + e^{-j\beta_2 L_2 - \frac{\alpha_2}{2} L_2} \right) \right|^2 \quad (3)$$

This equation represents the general form of an unbalanced MZI transfer function. However, for the purpose of this work, we can neglect the propagation loss relative to the constants α_1 and α_2 . Besides that, the propagation constants may also be considered equivalent in both branches, so that Equation 3 is simplified to:

$$I_0 = \frac{1}{2} I_i [1 + \cos(\beta\Delta L)] \quad (4)$$

The period of the peaks of the MZI transfer function, known as Free Spectral Range (FSR), is calculated by:

$$FSR = \frac{\lambda^2}{n_g(\lambda) \cdot \Delta L} \quad (5)$$

By measuring the FSR from the experimental interference pattern, we can calculate the group index n_g , assuming the central wavelength λ_0 and ΔL are known. This makes the MZI a valuable tool for passive characterization of waveguide dispersion and group index.

iii. Adjustable Splitter based on MZI with point-symmetric splitters

In real splitters, phases aren't equal at the outputs. Fortunately, it is possible to create an unbalanced MZI such that the phase differences are cancelled out. The approach is known as the "point symmetric" configuration, where the 2nd component is flipped in both horizontal and vertical axes, relative to the 1st one. This has the result of cancelling the phase differences.

For a certain splitting ratio $\frac{I_0}{I_i}$, e.g. 0.1 for 10%, using Equation 4 we can solve for the smallest path length difference ΔL that results in a broadband operation.

iv. Phase Splitter based on MZI with two ports

A phase splitter based on a Mach-Zehnder Interferometer (MZI) with two ports is a photonic device designed to split an optical signal into two outputs with a defined phase difference, typically 90° or 180° , depending on the design. In this project, a ΔL is introduced into one of the arms of the interferometer to introduce complementary outputs.

3. Modelling and Simulation

The waveguide chosen for design and simulation is a rectangular strip waveguide, with a default width of 500 nm and height of 220 nm. The 220nm-height is a typical value considered in the industry, and it has been widely used in wafer Foundries. The width of 500nm was chosen since there is experimental data (S-matrix) already available for the grating coupler and Y-branch models. All devices were designed for only TE polarization.

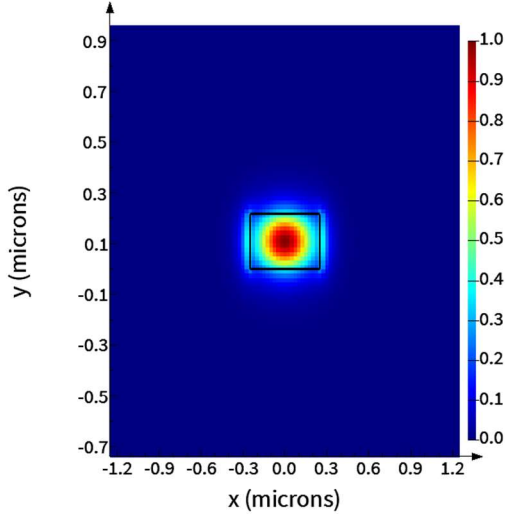


Figure 1 - Simulated waveguide mode profile (E intensity component).

$\hat{}$ mode #	effective index	wavelength (μm)	loss (dB/cm)	group index	TE polarization fraction (Ex)	waveguide TE/TM fraction (%)	effective area (μm^2)
1	$2.446821+1.249901e-09i$	1.55	0.00044009	4.203676+2.666268e-09i	98	76.12 / 81.96	0.190575
2	$1.768817+8.502992e-10i$	1.55	0.00029939	3.720462+4.417983e-09i	4	68.93 / 88.89	0.368811

Figure 2 - Simulated waveguide modes, with mode #1 being the TE fundamental mode, where effective and group index are calculated.

A modal analysis simulation was performed with the Lumerical MODE software, for the wavelength of 1550nm.

Next, a wavelength sweep was performed in the interval between 1500nm and 1600nm. After obtaining the modal analysis data, the effective index data was fit with respect to the wavelength. Considering a second-order Taylor expansion around the center wavelength lambda0 = 1.55 um, the effective index can be modelled as

$$n_{eff}(\lambda[\mu\text{m}]) = n_1 + n_2(\lambda - 1.55) + n_3(\lambda - 1.55)^2 \quad (6)$$

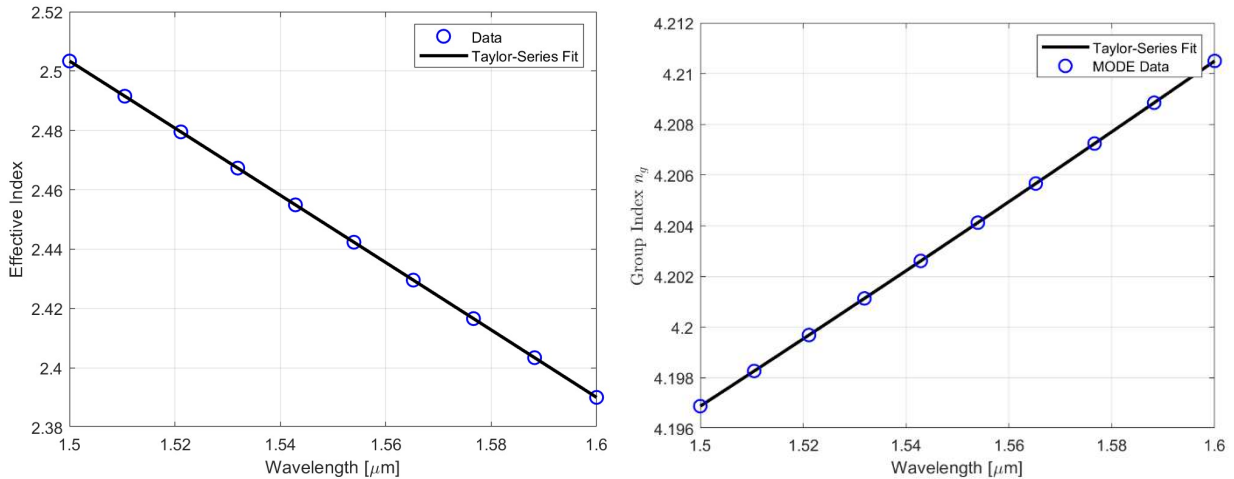


Figure 2 - Compact model of the TE mode, in terms of the effective index and group index. Markers indicate MODE data, and solid lines correspond to a Taylor-series approximation.

$$n_{eff} (\lambda[\mu m]) = 2.4468 - 1.1334 (\lambda - 1.55) - 0.0439 (\lambda - 1.55)^2 \quad (7)$$

The Taylor expansion parameters can also be converted to conventional parameters (effective index, group index, and dispersion) at the wavelength :

$$n_{eff} = n_1 = 2.4468 \quad (8)$$

$$n_g = n_1 - n_2 \cdot \lambda_0 = 4.2036 \quad (9)$$

$$D = -\frac{2 \cdot \lambda_0 \cdot n_3}{c} = 4.5429e - 10 \quad (10)$$

Next, corner analysis was performed to analyse its influence on group index variations. Manufacturing variability in photonic integrated circuits arises from inevitable imperfections during fabrication, such as deviations in waveguide widths, etching depths, or refractive index profiles. These variations can significantly impact the performance of sensitive components like MZIs. To ensure robust and reliable circuit behavior across different fabrication runs, corner analysis is essential. This involves simulating the circuit under a range of worst-case fabrication scenarios (process corners)—to evaluate its tolerance to variability. In this work, the wafers were provided by *Soitec*, Grenoble, France, and have a diameter of 6" and a Si thickness with average size of 219.2nm and a 6σ deviation of 23.4nm. Regarding the width of the waveguide, it depends on several factors of e-beam lithography, with variations within the +10/-30 nm range. Four corners were chosen due to these variations and results for the corner analysis and influence on effective and group index are shown in Figure 3.

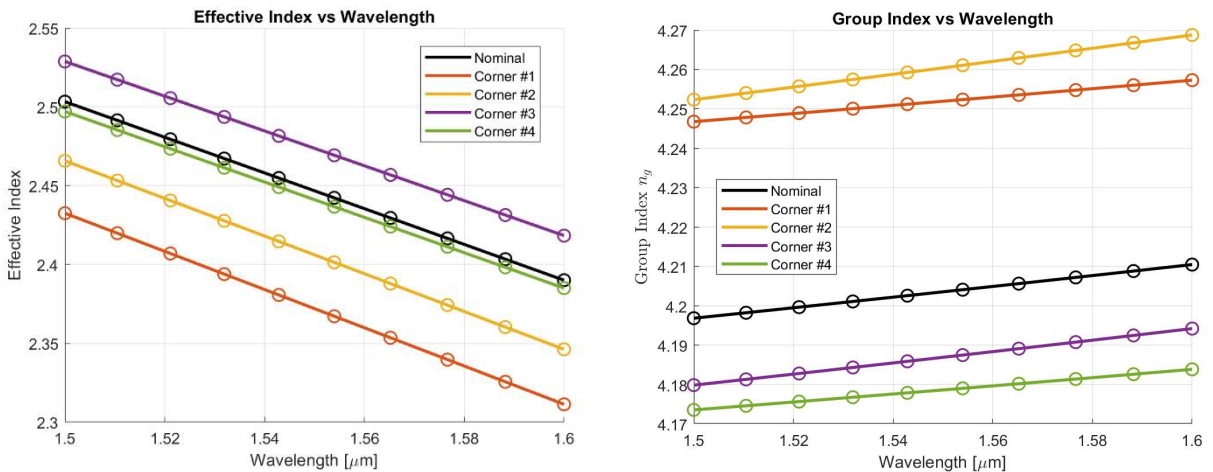


Figure 3 - Corner analysis of the a) effective index and b) group index, in the TE mode. Curves show the results for nominal design, 220nm-height x 500nm-width, and for the corner combinations, 219.2_3.9nm x 500 +10/-30nm.

Table 1 -Corner list waveguide dimensions.

Corners	Width (nm)	Thickness (nm)
#1	470	215.3
#2	470	223.1
#3	510	223.1
#4	510	215.3

Table 2 -Corners and Nominal's waveguide parameters comparison.

Corners	$n_{eff}@\lambda_0$	$n_g@\lambda_0$
Nominal	2.4468	4.2036
#1	2.3720	4.2520
#2	2.4061	4.2604
#3	2.4737	4.1869
#4	2.4411	4.1786

i. Layout

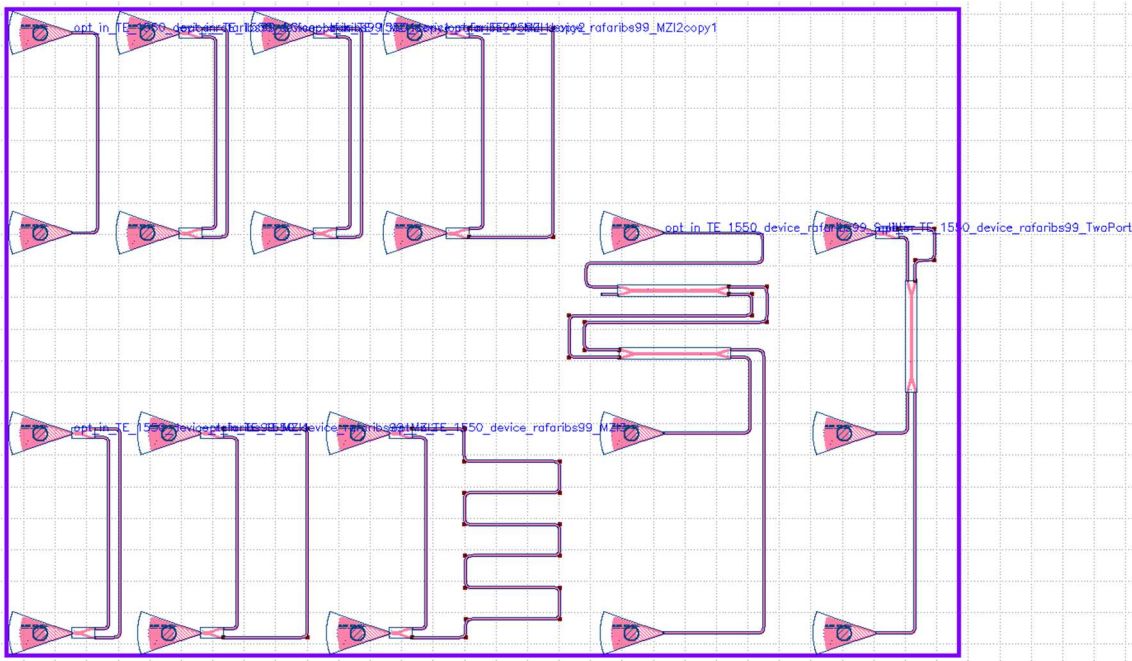


Figure 4 – Final version of the designed devices.

The design proposal was developed in KLayout software [12]. The final layout is presented in Figure 18, which contains 9 devices, 3 of them copies of the same design. The device list, along with its path length difference, is shown in Table 3.

Table 2 – List of the fabricated devices.

Label	Device	$\Delta L [\mu\text{m}]$
Loopback	Grating couplers connected	—
MZI1	MZI	25.44
MZI1copy1	MZI	25.44
MZI1copy2	MZI	25.44
MZI2	MZI	100
MZI2copy1	MZI	100
MZI3	MZI	402.62
Splitter	MZI Adjustable Splitter 20%/80%	0.09
TwoPort	MZI Phase Splitter 180°	32.12

Next, below is represented the simulated transmission spectrums of each unique device of the layout, done with Lumerical INTERCONNECT and the ebeam library.

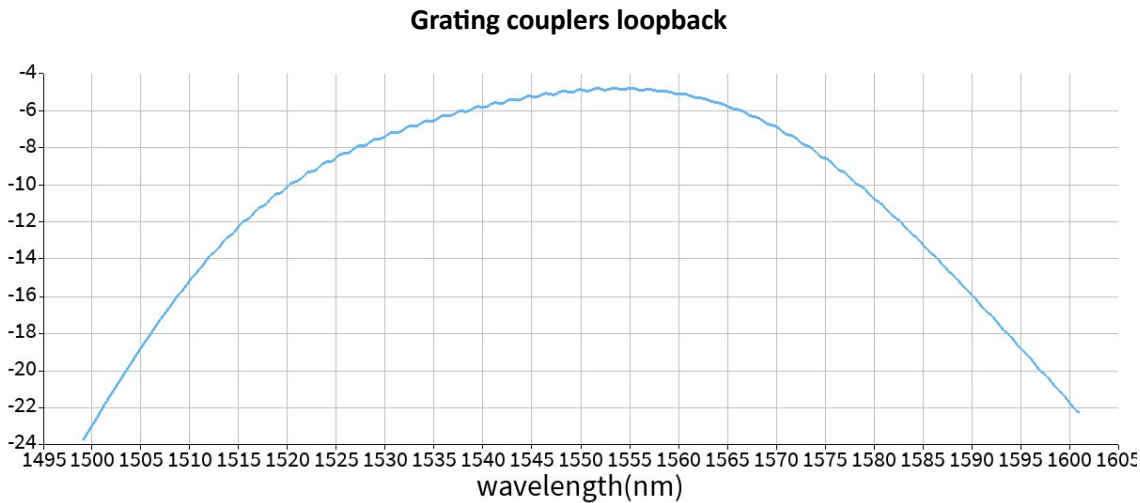


Figure 5 – Simulated Transmission spectrum for a loopback structure.

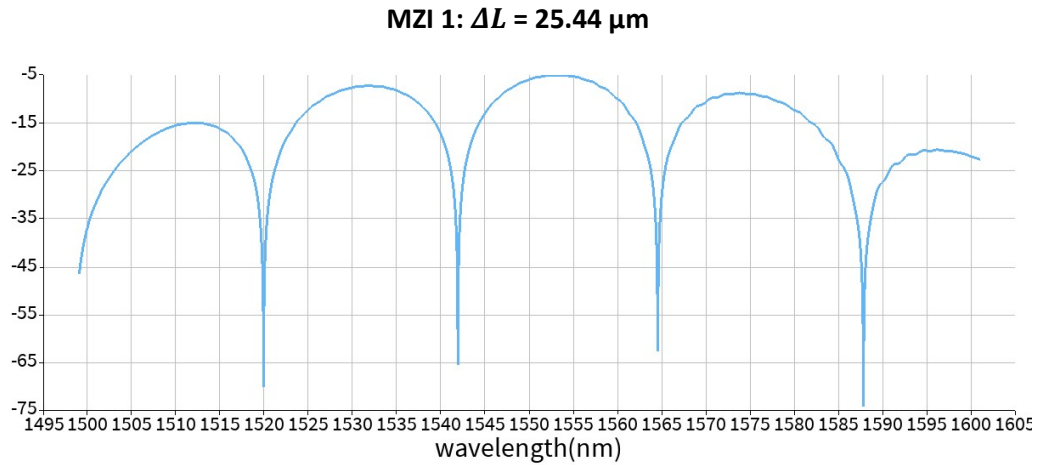


Figure 6 – Simulated Transmission spectrum for MZI1.

MZI 2: $\Delta L = 100 \mu\text{m}$

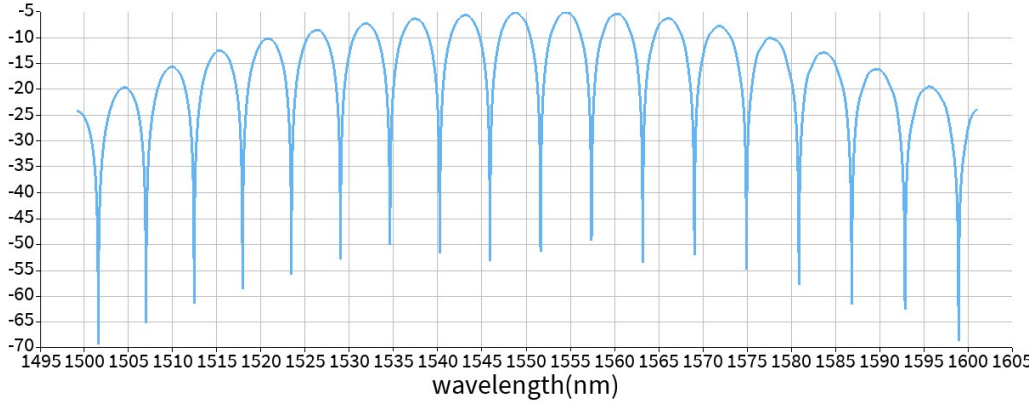


Figure 7 – Simulated Transmission spectrum for MZI2.

MZI 3: $\Delta L = 402.62 \mu\text{m}$

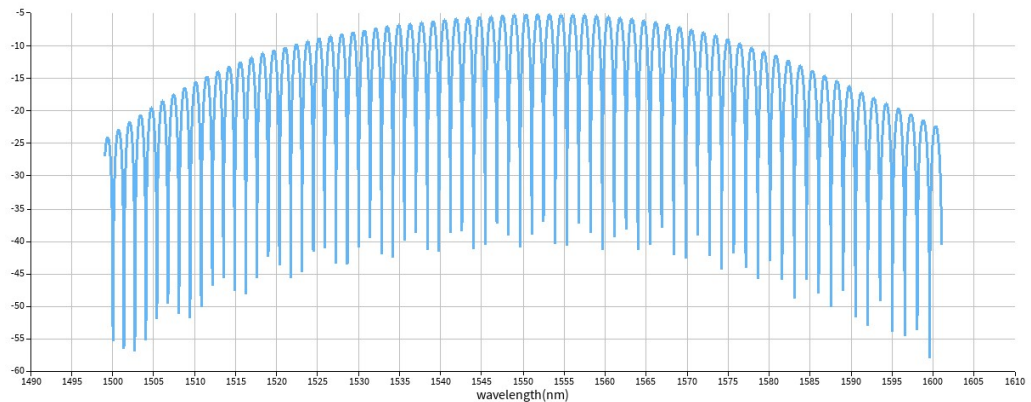


Figure 8 – Simulated Transmission spectrum for MZI3.

With knowledge of ΔL and n_g (from the compact model) for the central wavelength, it is possible to calculate the expected values for the FSR, with equation 11. Table 4 shows the expected FSR values for each MZI with different path length difference.

$$FSR = \frac{\lambda_0^2}{n_g \cdot \Delta L} \quad (11)$$

Table 3 – Expected FSR values for varying path length differences in MZIs.

Device	$\Delta L [\mu\text{m}]$	FSR expected [nm]
MZI1	25.44	22.47
MZI2	100	5.72
MZI3	402.62	1.42

Regarding the MZI adjustable splitter, a path length difference of 90 nm was designed to have a 20%/80% optical power distribution, where Figure 9 on the right side would show relatively constant lines with 0.2 and 0.8 for each port, with their sum contributing to the full optical power that entered the MZI. However, we have, at 1550 nm, 0.05 and 0.25, only portraying 30% total, hence 70% should corresponds to loss of the grating couplers and excess loss. Nonetheless, if we consider 0.3 to be the full optical power, $\frac{0.05}{0.3} = 0.166$ and $\frac{0.25}{0.3} = 0.833$, meaning that 16.67% of the power goes through one port and 83.3% goes through the other port.

MZI Adjustable Splitter approximately 20%/80%

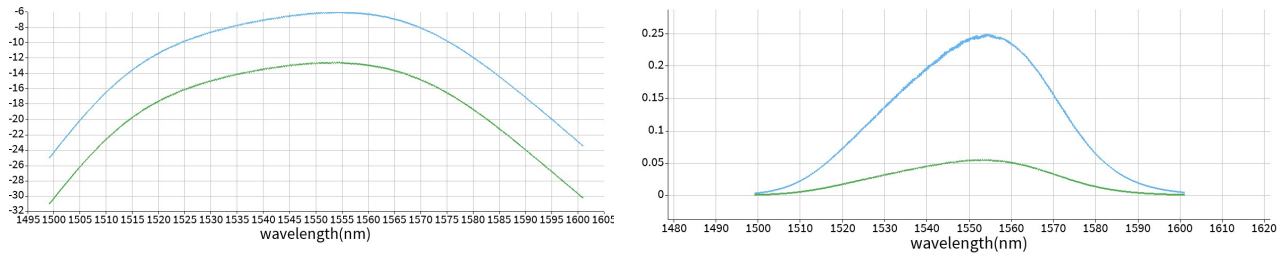


Figure 9 – Transmission spectrum in dB on the left, of both light signals. On the right, it is represented the squared absolute values of linear transmission, in dimensionless units.

MZI Phase Splitter 180°

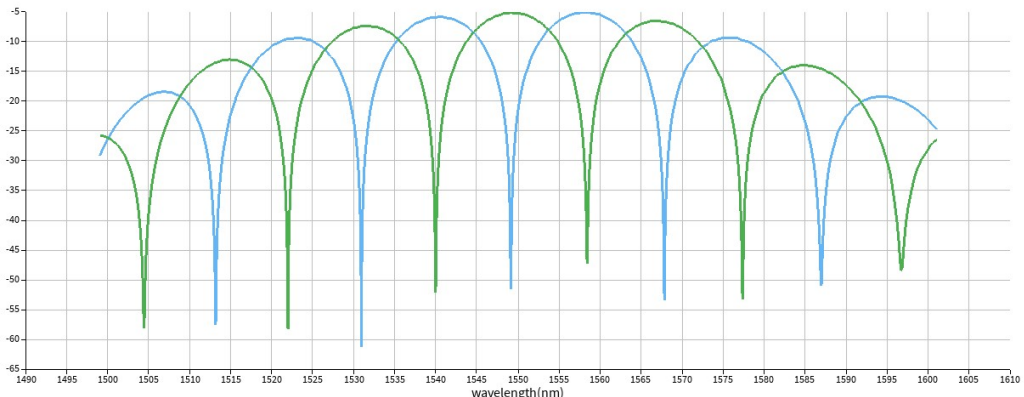


Figure 10 – Transmission spectrum of MZI ports with 180° phase difference.

4. Fabrication

i. Applied Nanotools, Inc. NanoSOI process:

The photonic devices were fabricated using the NanoSOI MPW fabrication process by Applied Nanotools Inc. (<http://www.appliednt.com/nanosoi>; Edmonton, Canada) which is based on direct-write 100 keV electron beam lithography technology. Silicon-on-insulator wafers of 200 mm diameter, 220 nm device thickness and 2 μm buffer oxide thickness are used as the base material for the fabrication. The wafer was pre-diced into square substrates with dimensions of 25x25 mm, and lines were scribed into the substrate backsides to facilitate easy separation into smaller chips once fabrication was complete. After an initial wafer clean using piranha solution (3:1 H₂SO₄:H₂O₂) for 15 minutes and water/IPA rinse, hydrogen silsesquioxane (HSQ) resist was spin-coated onto the substrate and heated to evaporate the solvent. The photonic devices were patterned using a Raith EBPG 5000+ electron beam instrument using a raster step size of 5 nm. The exposure dosage of the design was corrected for proximity effects that result from the

backscatter of electrons from exposure of nearby features. Shape writing order was optimized for efficient patterning and minimal beam drift. After the e-beam exposure and subsequent development with a tetramethylammonium sulfate (TMAH) solution, the devices were inspected optically for residues and/or defects. The chips were then mounted on a 4" handle wafer and underwent an anisotropic ICP-RIE etch process using chlorine after qualification of the etch rate. The resist was removed from the surface of the devices using a 10:1 buffer oxide wet etch, and the devices were inspected using a scanning electron microscope (SEM) to verify patterning and etch quality. A 2.2 μm oxide cladding was deposited using a plasma-enhanced chemical vapour deposition (PECVD) process based on tetraethyl orthosilicate (TEOS) at 300°C. Reflectometry measurements were performed throughout the process to verify the device layer, buffer oxide and cladding thicknesses before delivery.

5. Experimental Data

To characterize the devices, a custom-built automated test setup with automated control software written in Python was used. An Agilent 81600B tunable laser was used as the input source and Agilent 81635A optical power sensors as the output detectors. The wavelength was swept from 1500 to 1600 nm in 10 pm steps. A polarization maintaining (PM) fibre was used to maintain the polarization state of the light, to couple the TE polarization into the grating couplers. A polarization maintaining fibre array was used to couple light in/out of the chip.

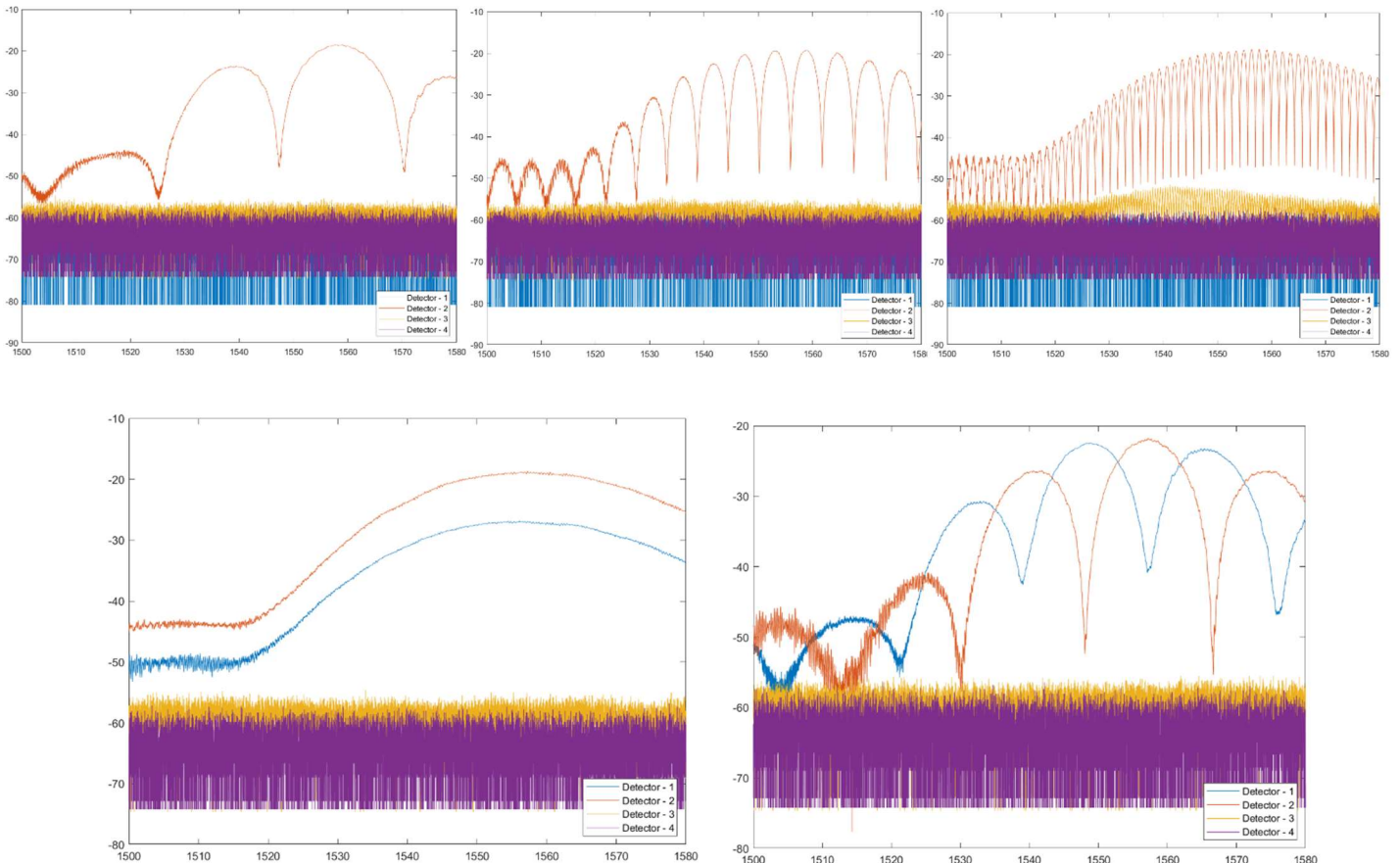


Figure 11– Raw data received from the Python-based setup, with the top row being the MZIs that vary the path length difference (MZI1, MZI2 and MZI3). On the bottom row, on the left is the Adjustable Splitter and on the right the Phase Splitter.

6. Analysis

First, a visual comparison of experimental results with simulations, for the different ΔL MZIs, was made. The experimental results are slightly shifted in regards to the simulated data, and also show higher losses, since the spectrum in every graph is about 10dB lower than the simulated data.

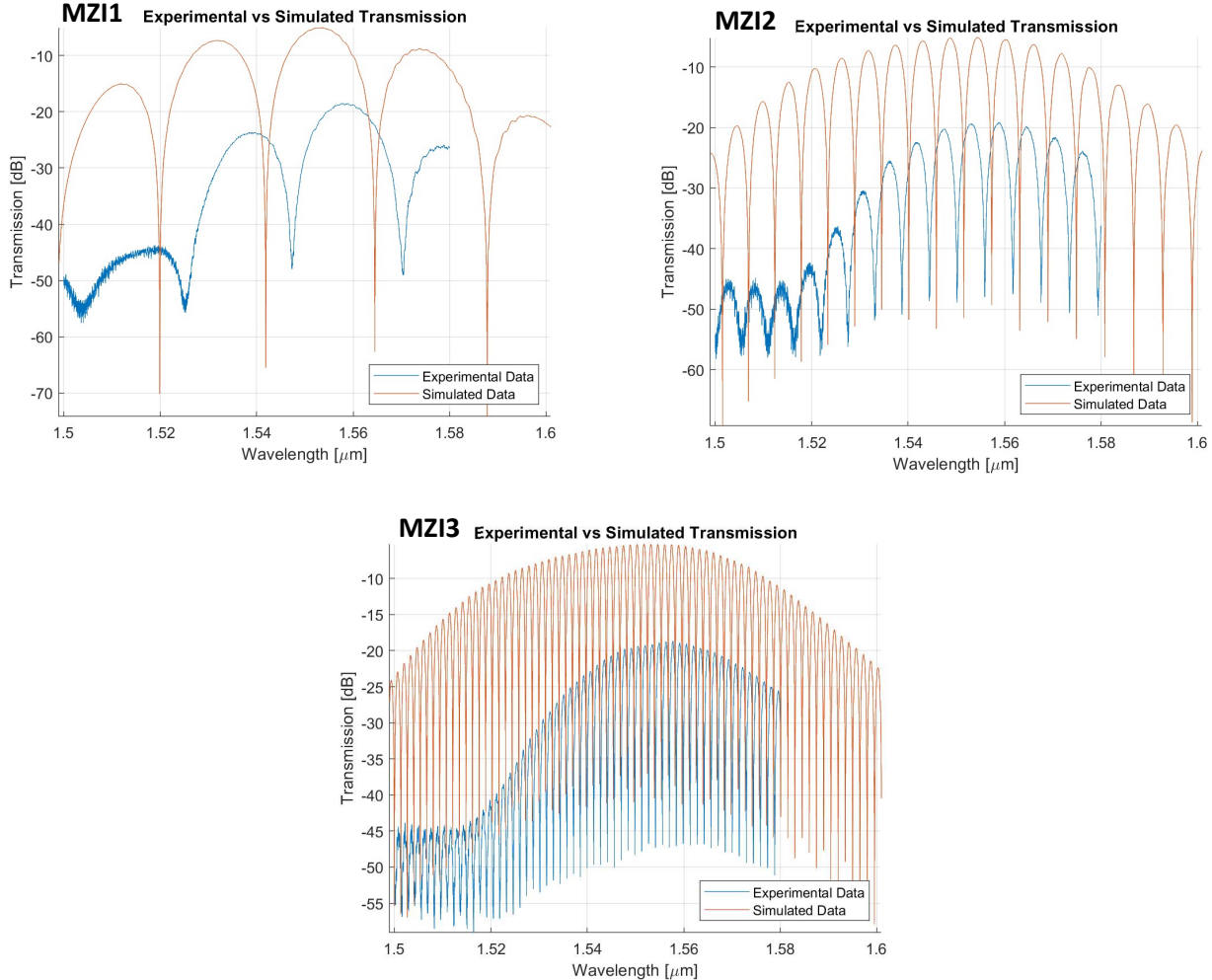


Figure 12– Comparison of experimental vs simulated transmission spectrums, for the different ΔL MZIs.

After plotting the data, baseline correction was applied with a polynomial fit (Figure 13-15) and most of the peaks are corrected and ready to move on to the next stage of finding peaks. In the following images of Figure 16, the pipeline to finding the FSR and waveguide parameters is shown for the MZI3.

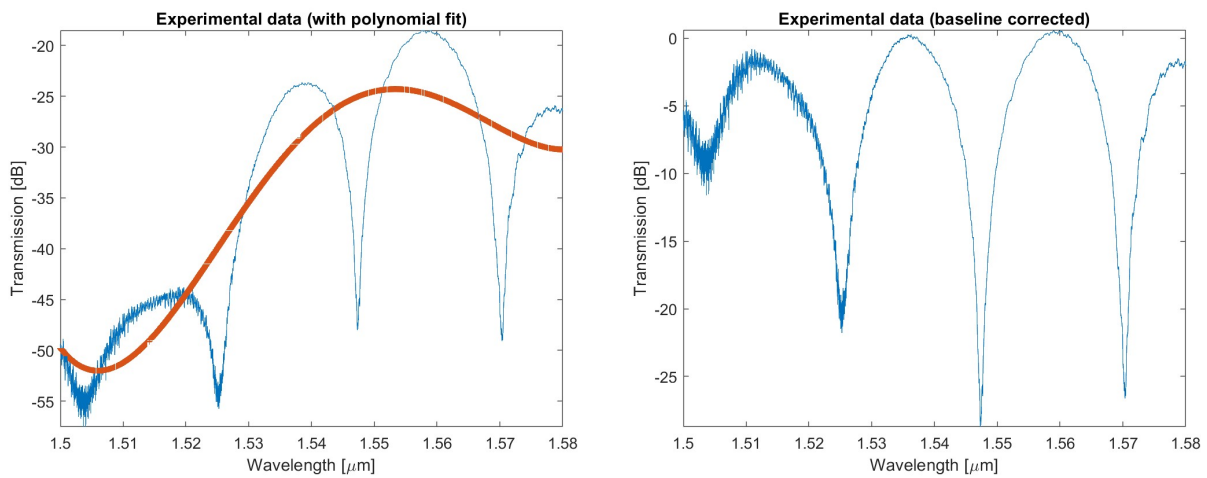


Figure 13 - Measured transmission spectrum on a Mach-Zehnder Interferometer MZI1 with a path length difference of 25.44 microns.

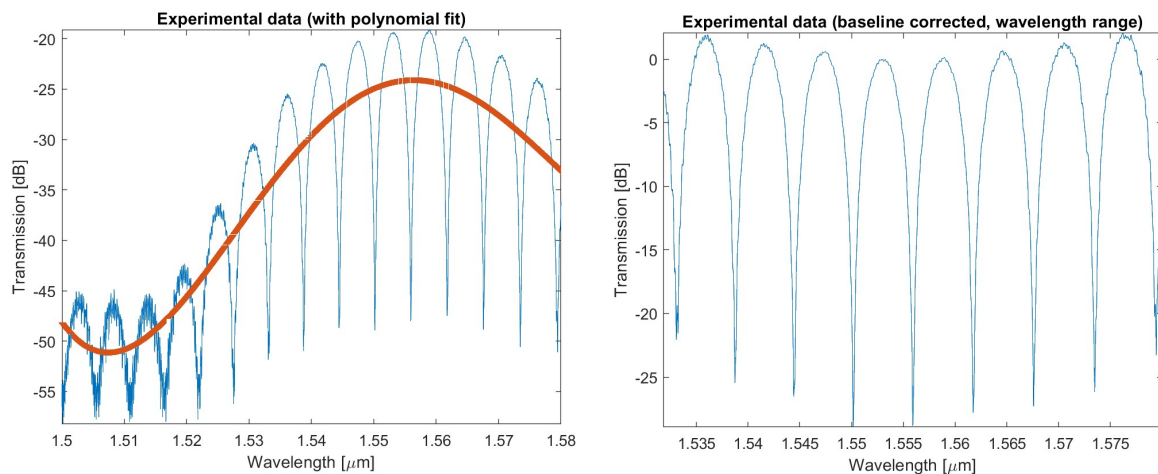


Figure 14-Measured transmission spectrum on a Mach-Zehnder Interferometer MZI 2 with a path length difference of 100 microns.

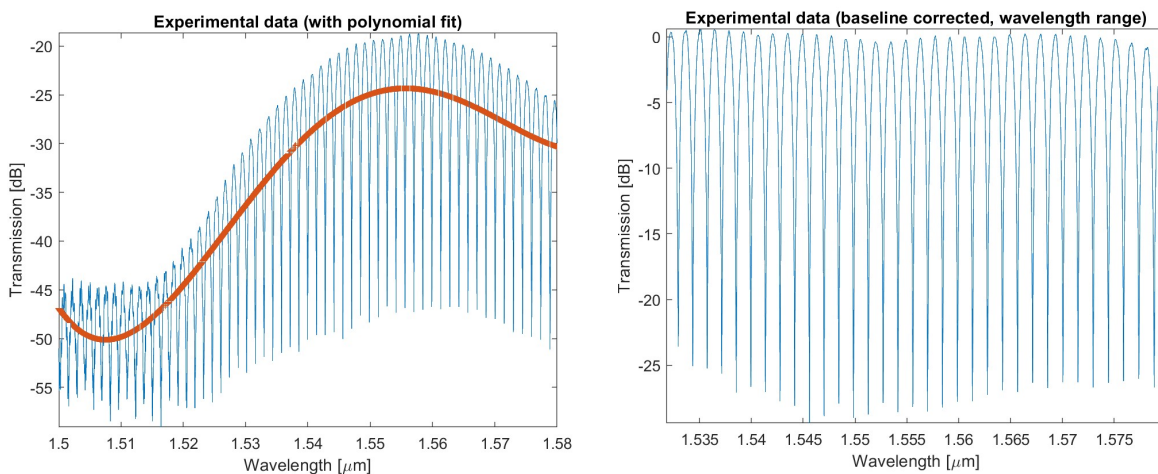


Figure 15 - Measured transmission spectrum on a Mach-Zehnder Interferometer MZI3 with a path length difference of 402.62 microns.

Process of getting n_g – findpeaks

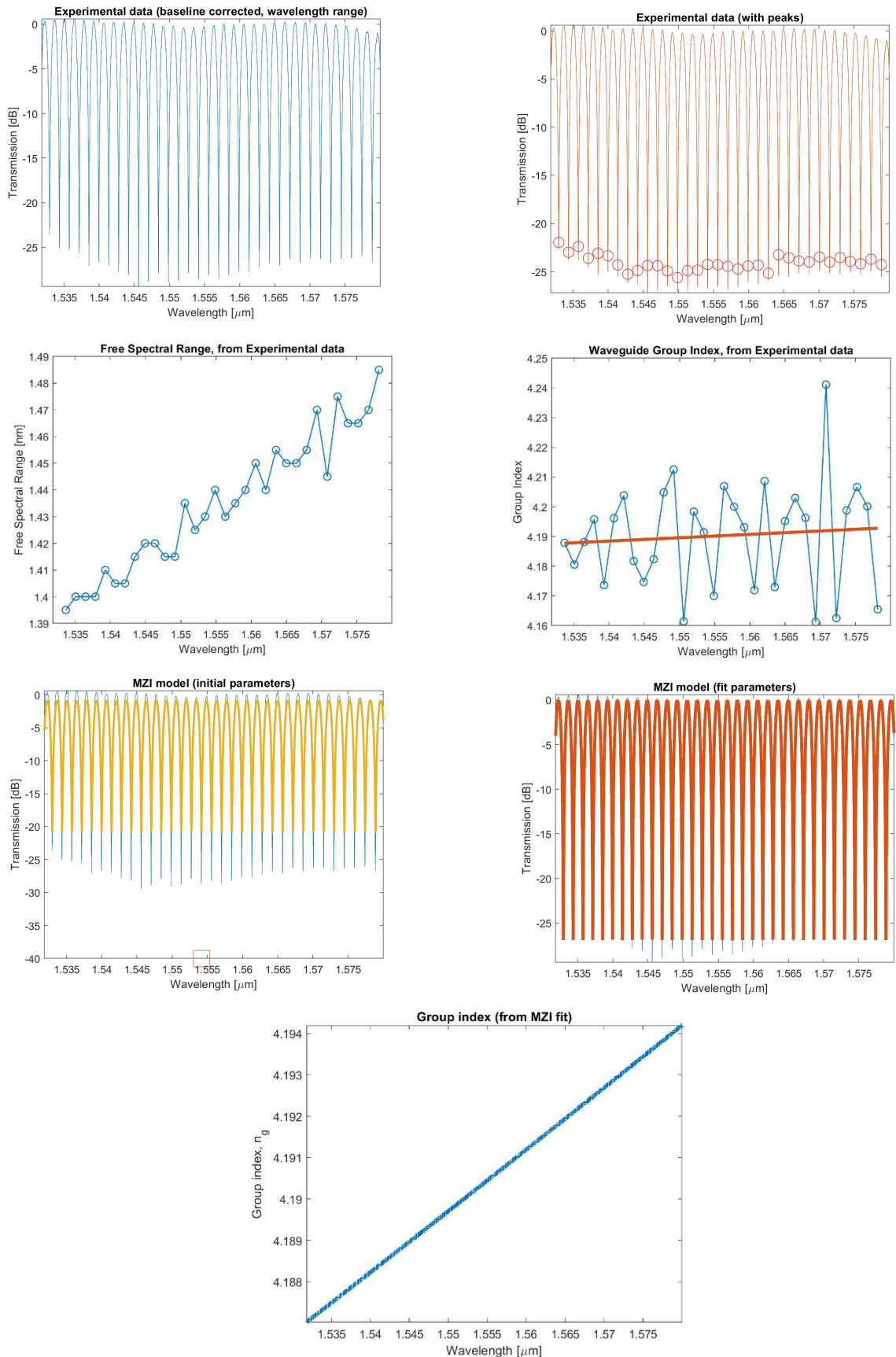


Figure 16 – Stages of findpeaks program, in order to have good initial guesses for the waveguide parameters, and reach optimal fitting to the MZI spectrum, to extract group index.

Extracting the waveguide parameters with the MZI3 gives a fit with a great $r^2 = 0.995$, a group index of $n_g = 4.1903$ at $1.55 \mu\text{m}$, a FSR = 1.407 nm and n_g experimental data that, despite not ideal to the simulated, lies within the range determined by the corner analysis, as seen in the following graph.

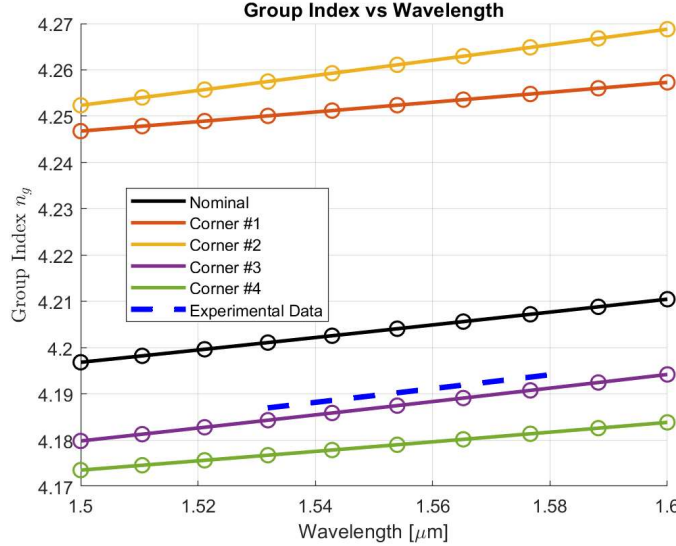


Figure 17 - Corner analysis of the group index and experimental data lies within the manufacturing variability range.

Table 4 -Error of the FSR estimation for each MZI with different ΔL .

Device	$\Delta L [\mu\text{m}]$	FSR expected [nm]	Experimental FSR [nm]	Error (%)
MZI1	25.44	22.47	22.23	1.07
MZI2	100	5.72	5.66	1.05
MZI3	402.62	1.42	1.41	0.70

Table 5 - Error of the n_g estimation for each MZI with different ΔL .

Device	Expected n_g (1550 nm)	Extracted n_g	Error (%)
MZI1	4.2036	4.1633	0.96%
MZI2	4.2036	4.1794	0.58%
MZI3	4.2036	4.1903	0.32%

For MZI1, unexpectedly the extracted group index is lower than the minimum corner analysis (4.1786), possibly due to the low number of fringes/peaks that the MZI has, a low amount of data usually isn't enough to get the whole picture, and as we progress from MZI1 to MZI3, with more peaks, the results get much better. Another possibility could be the first band that appear on MZI1, between 1500-1530 nm, it appears quite noisy and diminished in amplitude, suggesting

that in future similar tasks, those noisier bands should not be considered in the range for calculating the group index.

Lastly, about the Adjustable Splitter 20/80% MZI, after converting the data to a linear transmission and squaring its values and correcting the transmission after subtracting the background of the gratings loopback structure, we obtain this graph below with approximately 82% and 13.5% at 1550 nm. It is relatively close to the 16.6% predicted by the simulated data.

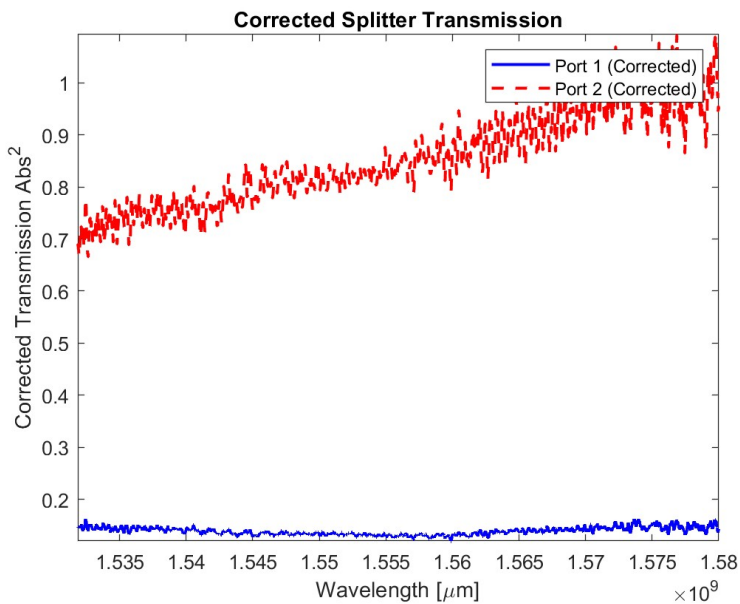


Figure 18 – Adjustable Splitter Linear Transmission, with absolute squared values, and corrected from the loopback structure to try and isolate power contributions.

8. Conclusion

This report described the main steps to design, simulate, and analyze various MZI configurations to understand their optical behavior and compare performance with expected response. The group index and the FSR were the main merit figures used for comparison between the designed and fabricated versions. The FSR had a low error percentage, while for the group index, despite the error not being very high, the group index value of MZI1 did drop below the minimum corner analysis, suggesting that new corner values should be applied or that some process of the analysis could be improved, such as applying autocorrelation or applying the baseline correction of the loopback grating couple structure, instead of a polynomial, which can be arbitrary.

9. Acknowledgements

I acknowledge the edX UBCx Phot1x Silicon Photonics Design, Fabrication and Data Analysis course, which is supported by the Natural Sciences and Engineering Research Council of Canada

(NSERC) Silicon Electronic-Photonic Integrated Circuits (SiEPIC) Program. The devices were fabricated by Richard Bojko at the University of Washington Washington Nanofabrication Facility, part of the National Science Foundation's National Nanotechnology Infrastructure Network (NNIN), and Cameron Horvath at Applied Nanotools, Inc. Enxiao Luan performed the measurements at The University of British Columbia. We acknowledge Lumerical Solutions, Inc., Mathworks, Mentor Graphics, Python, and KLayout for the design software.